Phys. Status Solidi RRL **11**, No. 2, 1600426 (2017) / **DOI** 10.1002/pssr.201600426

pss +++rapid research letters+++
www.pss-rapid.com

Microstructural identification of Cu in solar cells sensitive to light-induced degradation

Tabea Luka[*,1,2], **Marko Turek**[1], **Stephan Großer**[1], **and Christian Hagendorf**[1]

[1] Fraunhofer Center for Silicon-Photovoltaics CSP, 06120 Halle (Saale), Germany
[2] Anhalt University of Applied Sciences, 06366 Köthen (Anhalt), Germany

Received 9 December 2016, revised 21 December 2016, accepted 23 December 2016
Published online 9 January 2017

Keywords solar cells, PERC, copper, light-induced degradation

* Corresponding author: e-mail tabea.luka@csp.fraunhofer.de, Phone: + 49 345 5589-5130, Fax: + 49 345 5589-101

Light-induced degradation (mc-LID or LeTID) can lead to a severe efficiency loss in multi-crystalline solar cells. The underlying mechanism clearly distinguishes from known mechanisms as B-O-LID and Fe-B-LID. Various defect models have been suggested for mc-LID mainly based on metal impurities, including Cu which is known to cause light-induced degradation. We investigate mc-LID sensitive PERC cells that show an efficiency degradation of 15%$_{rel}$. The weaker degradation of the grain boundaries (GBs) typical for mc-LID is identified and further investigated from front and rear side with respect to recombination activities. The combination of local electrical measurements (LBIC), target preparation (REM, FIB) and element analysis (EDX, TEM) unveil Cu-containing precipitates at the rear side of the solar cells. They accumulate at grain boundaries and at the rear surface of the Si-bulk material where the passivation stack is damaged. We conclude that Cu originates from the cell material and discuss its relation to mc-LID.

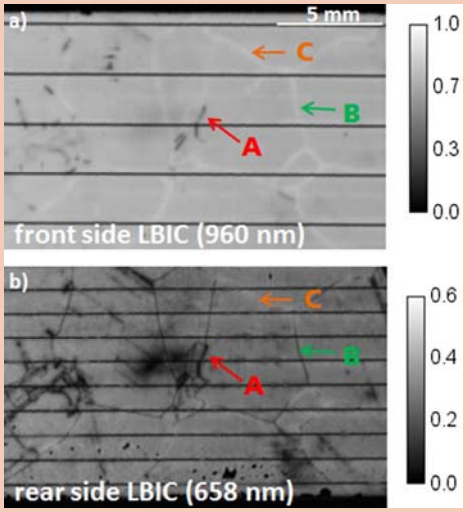

LBIC mapping (EQE at fixed wavelength) of a degraded mc-Si PERC cell from front and rear side results in qualitatively different appearance of GBs.

1 Introduction In 2012, Ramspeck et al. reported a new light-induced degradation mechanism (mc-LID also referred to as LeTID) that can cause a severe efficiency loss of multi-crystalline solar cells [1]. PERC cells are mainly affected showing an efficiency reduction of more than 10%$_{rel}$ in some cases [1, 2]. This degradation can be reduced by adapting the cell process [2, 3]. However, this implies a narrowing of the process window leaving fewer options for the optimization of cell properties. Detailed analysis of the electrical losses based on quantum efficiency measurements (EQE) has shown that mc-LID mainly affects the bulk material while the rear side might also be affected to some minor extent [4]. Spatially resolved current measurements (LBIC) further indicate that grain boundaries (GBs) show a less pronounced degradation while mc-LID appears rather homogeneously throughout intra-grain regions of the solar cells [5, 6]. This leads to the conclusion that point defects are involved in mc-LID [5]. However, the particular defect type could not be identified, yet. At present, B-O-LID and Fe-B-LID

could be excluded due to their different defect kinetics with respect to minority carrier injection and temperature [1, 2, 7]. Among other defect complexes being discussed as degradation sources, Cu plays a special role due to its positive charge state and its diffusion and precipitation behavior [8–10]. The role of thin amorphous oxide layers, such as the rear side passivation stack of PERC cells, as Cu-diffusion barriers has been shown previously [9, 11].

In order to clarify mc-LID related defect formation and underlying mechanisms, this paper presents latest results on microstructural root cause diagnostics at industrial, mc-Si PERC solar cells. To this aim, PERC cells showing the kinetics known for mc-LID are investigated. We classify the grain boundaries by the recombination properties appearing during front and rear side measurements. High-resolution LBIC in combination with target preparation and microstructure analysis is applied to localize the Cu containing precipitates at the rear of mc-LID sensitive PERC solar cells.

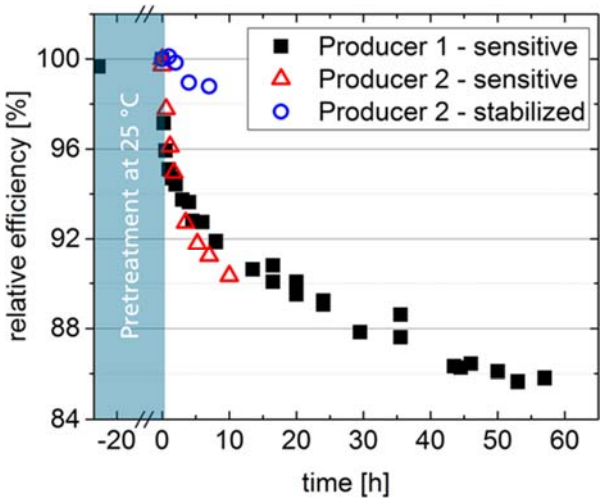

Figure 1 Solar cell efficiency decreasing over time during 25 °C pre-treatment and 75 °C degradation phase at 1 sun illumination.

2 Experimental The investigated samples are industrially produced mc-Si PERC solar cells from different cell producers. The degradation has been carried out at 1 sun and at elevated temperature of 75 ± 5 °C using an LED based test setup [12] leading to accelerated mc-LID degradation. Throughout degradation, electrical cell parameters have been monitored under standard test conditions using a solar cell loss analysis tool (LOANA) and the defect kinetics has been quantified [13]. A pre-treatment was performed at the sample from producer 1 by illuminating the solar cell for 24 h at 25 ± 2 °C and 1 sun to value the influence of other (non mc-LID) degradation mechanisms such as BO-defect activation or FeB dissociation.

Subsequently, the aluminum metallization layer at the solar cell rear side was mechanically lifted-off revealing the passivated rear side of the solar cell. The samples were investigated with LBIC at 6 different wavelengths between 405 nm and 980 nm (LOANA) at an injection level of approximately 10^{14} cm^{-3}. High-resolution LBIC (µLBIC) was carried out by an in-house developed system using a LSM700 from Zeiss equipped with a DISS5/LBIC system from point electronic. Scanning electron microscopy (SEM) using a Hitachi SU70 was utilized for detailed inspection of the microstructure of defect sites. The SEM is equipped with an EDX detector by EDAX to measure their chemical composition, with a detection limit in the rage of 0.1–1 atomic percent. Cross sections of particles were obtained using a focused ion beam (FIB) AURIGA from ZEISS. In this dual beam machine the FIB cross sections could be investigated directly by included SEM. More detailed investigations used high resolution (scanning) transmission electron microscope FEI TEM/STEM Tecnai G2 F20 with equipped EDX detector.

3 Results and discussion

3.1 mc-LID kinetics and loss analysis The conditions of the 24 h pre-treatment degradation at room temperature are chosen such that almost all BO- and Sponge-LID-related defects are activated and FeB pairs are dissociated [13–15]. Nevertheless, the efficiency of the investigated solar cells from producer 1 changed less than $0.5\%_{rel}$ during the pre-treatment (Fig. 1). Thus, degradation mechanisms as BO activation, FeB dissociation, and Sponge-LID have a minor effect on these samples and can be neglected. The subsequent degradation at 75 °C leads to the typical lateral appearance known for mc-LID (abstract figure) with enhanced intra-grain degradation and less affected grain boundaries [5, 6, 16]. The efficiency drops almost $15\%_{rel}$ and reaches a minimum after about 60 h of light soaking at 75 °C, see Fig. 1. The degradation rate at 75 °C is of the order of 2×10^{-5} s^{-1} which compares to approximately 3×10^{-3} s^{-1} for BO-LID [13] and 7 s^{-1} at room temperature for FeB-LID with low FeB concentration [14].

The sensitive cells of producer 1 and 2 show a comparable degradation behavior which indicates the same underlying degradation mechanism (mc-LID). The stabilized solar cell shows only a slight degradation of approximately $1\%_{rel}$ (Fig. 1), which might be caused by other degradation effects. The typical appearance of GBs with higher-than-average lifetime does not occur for stabilized in-sensitve cells [5].

3.2 Spatially resolved electrical analysis The degraded samples are investigated from the front and rear side to get a more profound understanding of lateral variations in bulk lifetime and rear passivation quality. The comparison of the spatial resolved LBIC measurements of both sides, shown in abstract figure for solar cell from producer 2, reveals a qualitatively different appearance at various grain boundaries leading to the following classification: GB-type A shows a high recombination from the front and from the rear. They are decorated grain boundaries where non-mc-LID recombination mechanisms are dominant. Thus, they do not change significantly during

degradation [5]. GB-type B and C show the typical behavior of mc-LID when measured from the front side at a long wavelength of 960 nm (corresponding to an absorption length of 75 µm): a reduced degradation at these grain boundaries is observed compared to intra-grain regions. Rear-side LBIC measurements with a relatively low wavelength of 658 nm (corresponding to an absorption length of 4 µm) distinguish the two types. Type B shows a pronounced recombination in the rear-side LBIC. When the rear-side LBIC is performed with longer excitation wavelengths, this effect is less pronounced. Therefore, the reduced rear-side LBIC-signal at GB-type B can be assigned to a locally increased rear surface recombination. Thus, the different appearance of GB-type B from the front and rear side, respectively, can be explained by a comparatively high local bulk lifetime combined with a high rear surface recombination. At GB-type C, no intensified rear recombination is detected and investigations from the rear as well as from the front show a comparatively better grain boundary than intra-grain regions. In order to analyze the different rear side behavior of GB-types B and C, respectively, a local microstructural characterization with increased spatial resolution has been performed. At a mc-LID stabilized sample from producer 2, no enhanced rear recombination at GBs and no change in local electrical properties due to mc-LID were detected.

3.3 Microstructural characterization Figure 2(a, b) shows µLBIC images obtained from the rear side of a degraded PERC solar cell from producer 2. We have employed a relatively short excitation wavelength of 639 nm to localize regions with increased rear surface recombination. The exposed rear side exhibits recombination-active and -inactive areas at grain boundaries that appear entirely recombination-inactive from the front side (GB-type B in abstract figure). A bright area of reduced recombination surrounds these grain boundaries. This observation is an indication for a gettering process by the grain boundary. Furthermore, recombination-active intra-grain sites have been found (see Fig. 2(b), marked with A as dashed circles). The specific halo of the µm-sized recombination side allows a precise distinction from Al-sphere residuals (marked with B as solid circles) which exhibit a well-defined shape without a halo.

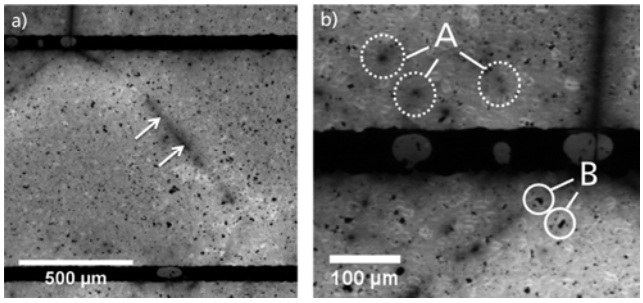

Figure 2 µLBIC images (EQE at 639 nm in arbitrary units) from the rear side (producer 2) with recombination active areas at (a) grain boundaries (arrows) and (b) within intra-grain regions aside from grain boundaries (circled). The dark spots (B, solid circles) are residuals from the back-contact metallization.

Microstructure information of the recombination sites is obtained by SEM and EDX analysis performed at the exposed passivated rear surface. Figure 3(a) shows a SEM image at a recombination active grain boundary which proceeds horizontally in the image. An EDX mapping at this position (Fig. 3(b)), unveils copper containing precipitates located at the grain boundary which corresponds to the visible precipitates in the SEM image. A direct correlation between the precipitates and the recombination activity at the rear side could not be established by SEM/EDX. This can be caused by limited sensitivity of EDX. In contrast to the grain boundaries, a clear correlation was found between intra-grain recombination sites and precipitates. Figure 3(c) shows an SEM image of an intra-grain recombination site as an example of a precipitation at the surface confirmed by an EDX-map of Cu and N (Fig. 3(d)). The size of the precipitates is in the range of around 100 nm. Furthermore, we found by EDX that the appearance of precipitates was restricted to areas with damaged passivation stack (missing N signal in EDX). This absent passivation layer distinguishes these intra-grain regions from the grain-boundaries with Cu precipitates. A further experi-

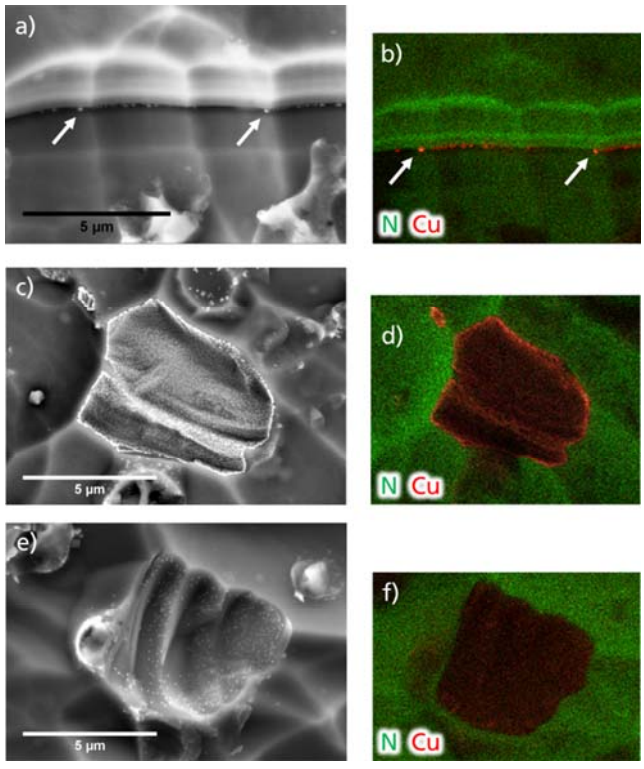

Figure 3 SEM micrographs at a grain boundary (a) and at a damaged rear surface passivation (c) and related EDX-map overlays for copper (red) and nitrogen (green) in (b, d) for a mc-LID degraded PERC cell (producer 2). (e) SEM micrograph and (f) EDX-map overlay of Cu (red) and N (green) for a mc-LID stabilized cell (color levels not on absolute scales).

ment performed on a solar cell from a LID-stabilized cell process results in and differs clearly by a lower concentration of Cu-containing precipitates at intra-grain recombination sites (Fig. 3(e, f)). The EDX map of Cu in (Fig. 3(f)) is dominated by background noise due to the low precipitate concentration. The presented images of a sensitive solar cell are all taken from the same sample from producer 2. The same qualitative results at another sensitive solar cell sample from producer 2 and from producer 1 were obtained, regarding an enhanced rear recombination at grain boundaries and at areas with locally damaged passivation. Also, the formation of Cu-containing precipitates was observed at the solar cells rear side. However, there seems to be some variations related to the amount of Cu detected.

3.4 High resolution analysis of microstructure and stoichiometry A cross section has been prepared precisely at the position of a Cu-containing precipitate located at a grain boundary. Subsequent TEM analysis shown in Fig. 4(a) reveals a precipitate on top of the passivation stack at a grain boundary (marked). A form-fit contact of the precipitate to the surface topography (trench) can be found. The TEM data unveil a filled "channel" connecting the precipitate and the Si-substrate. Furthermore, a defect can be seen located close to the grain boundary. Figure 4(b) shows an EDX spectrum acquired at the position of the precipitate. It confirms that it is a copper silicide. A first quantitative analysis results in a stoichiometry of CuSi which is assigned to a metastable phase at room temperature [17]. The measured stoichiometry differs from the expected Cu_3Si phase, reported by Seibt et al. [18] and indicates the need for more detailed investigation on the found precipitates. The other found elements (Pt, Ga, Au, C and O) originate from the sample preparation and mounting.

The observation of the copper silicide precipitates on top of the passivation layer connected to the Si-bulk material by a channel, Fig. 4(a), together with the observation of Cu-containing precipitate colonies at areas of damaged surface passivation directly on top of the Si-bulk material, Fig. 3(c–f), leads to the conclusion that the Cu originates from the Si-material.

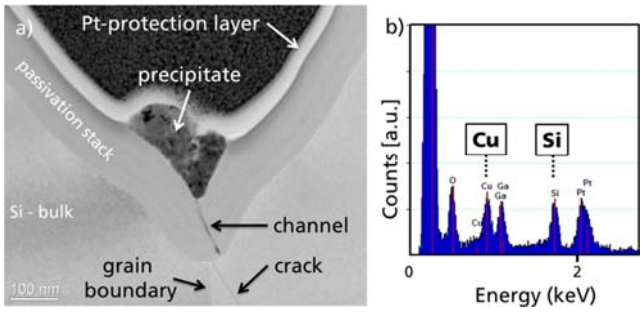

Figure 4 (a) TEM micrograph of a copper containing precipitate at a grain boundary and (b) an EDX point spectrum of the precipitate.

4 Conclusions Multi-crystalline silicon solar cells with passivated rear side (PERC cells) were investigated on their LID sensitivity and the lateral appearance of the degradation. It was found that the investigated samples show no significant BO-, Sponge-, or FeB-LID. The determined LID kinetics distinguishes from what is known for BO activation and FeB dissociation. The samples show strong mc-LID degradation with an efficiency loss of almost $15\%_{rel}$ that mainly affects the solar cell bulk while a contribution of the rear passivation cannot be excluded. Different types of grain boundaries were identified through their front and rear side recombination properties after degradation. GB-type A was identified as completely decorated grain boundary of high recombination which does not change by mc-LID. GB-types B and C are less effected by mc-LID in comparison to the intra-grain region when inspected from the front side which coincides with previous findings for mc-LID.

At grain boundaries of GB-type B, the rear surface recombination is locally increased which is not the case at GB-type C. A possible root cause is detected by TEM images of GB-type B exhibiting copper silicide precipitates on top of the passivation layer. The underlying passivation stack shows a channel-like structure which is most likely filled with a copper-silicide. Furthermore, areas with high rear surface recombination were observed at intra-grain regions. Here, Cu containing precipitates were detected together with a locally damaged passivation. These two observations indicate that Cu originates from the Si material. Furthermore, Cu precipitation supports a damage of the rear passivation layer and is particularly pronounced in mc-LID sensitive solar cells. It is unclear to which extend the precipitates form during degradation, or if they are present even before degradation. However, due to its strong lateral and vertical confinement, reduction of the rear surface quality has a minor impact on the efficiency degradation. The severe efficiency loss is caused by homogeneous degradation of the Si bulk material through carrier induced activation of point defects reflected by its widespread appearance and the high recombination activity.

A direct correlation between the observed copper silicide precipitate formation and the Si bulk material degradation could not be established, yet. However, Cu contaminations should be taken into account for playing a root cause role in mc-LID in further investigations. As described in previous works on Cu-LID, the major properties of Cu contaminations in Si are its high diffusivity and low solubility at low temperatures leading to pronounced precipitate formation and out-diffusion. Furthermore, the impact of thin amorphous oxide layers as efficient diffusion barriers that inhibit Cu gettering into the metallic rear contact has also been presented previously. Thus, our findings could explain the different degradation behavior between Al-BSF solar cells and PERC solar cells, respectively. The PERC solar cell design, e.g. the absence of Al-BSF gettering, can have a detrimental impact on temperature and minority charge carrier dependent formation of Cu defect complexes and Cu precipitation in the mc-Si bulk material.

Acknowledgements We thank our colleagues Susanne Richter, Sina Swatek, Martina Werner, and Stefan Eiternick for sample preparation, TEM analysis, and support by experiments. Furthermore, we thank the German Federal Ministry for Commerce and Energy and the industry partners within the research cluster "SolarLIFE" (contract 0325763 D) for the financial support and the Federal Ministry of Education and Research for the financial support within the joined research graduate school "StrukturSolar II" (03SF0417 A).

References

[1] K. Ramspeck et al., Proceedings of the 27th EU-PVSEC, 861–865 (2012), DOI: 10.4229/27thEUPVSEC2012-2DO.3.4
[2] F. Kersten et al., Sol. Energy Mater. Sol. Cells **142**, 83–86 (2015).
[3] C. E. Chan et al., IEEE J. Photovolt. **6**, 1473–1479 (2016).
[4] T. Luka et al., Proceedings of the 31 EU-PVSEC, 826–828 (2015), DOI: 10.4229/EUPVSEC20152015-2BV.8.12
[5] T. Luka et al., Sol. Energy Mater. Sol. Cells **158**, 43–49 (2016).
[6] M. Selinger et al., Energy Proc. **92**, 867–872 (2016).
[7] F. Fertig, K. Krauß, and S. Rein, Phys. Status Solidi RRL **9**(1), 41–46 (2015).
[8] K. Nakayashiki et al., IEEE J. Photovolt. **6**(4), 860–868 (2016).
[9] A. A. Istratov and E. R. Weber, J. Electrochem. Soc. **149**(1), G21–G30 (2002).
[10] J. Lindroos and H. Savin, Sol. Energy Mater. Sol. Cells **147**, 115–126, (2016).
[11] M. B. Shabani et al., J. Electrochem. Soc. **143**, 2025–2029 (1996).
[12] Patent pending, no. 15200094.9–1555.
[13] K. Bothe and J. Schmidt, J. Appl. Phys. **99**, 013701 (2006).
[14] L. J. Geerligs and D. Macdonald, Appl. Phys. Lett. **85**, 5227 (2004).
[15] K. Sporleder et al., Proceedings of the 32th EU-PVSEC, 883–885 (2016).
[16] A. Zuschlag, D. Skorka, and G. Hahn, 32nd EU-PVSEC (2016), DOI: 10.1002/pip.2832.
[17] G. Das, J. Appl. Phys. **44**, 4459 (1973).
[18] M. Seibt et al., Phys. Status Solidi A **171**, 301–310 (1999).